Title

Processes controlling δ 7Li in rivers illuminated by study of streams and groundwaters draining basalts

Authors

Liu, Xiao-Ming
Wanner, Christoph
Rudnick, Roberta L
et al.

Publication Date

2015

DOI

10.1016/j.epsl.2014.10.032

Peer reviewed

Earth and Planetary Science Letters 409 (2015) 212–224

Contents lists available at ScienceDirect

Earth and Planetary Science Letters

www.elsevier.com/locate/epsl

Processes controlling δ^7Li in rivers illuminated by study of streams and groundwaters draining basalts

Xiao-Ming Liu [a,b,*], Christoph Wanner [c], Roberta L. Rudnick [a], William F. McDonough [a]

[a] Department of Geology, University of Maryland, College Park, College Park, MD, USA
[b] Geophysical Lab, Carnegie Institute of Washington, Washington, DC, USA
[c] Earth Sciences Division, Lawrence Berkeley National Laboratory, Berkeley, CA, USA

ARTICLE INFO

Article history:
Received 28 February 2014
Received in revised form 23 September 2014
Accepted 18 October 2014
Available online 19 November 2014
Editor: J. Lynch-Stieglitz

Keywords:
lithium isotopes
chemical weathering
rivers and groundwaters
reactive transport modeling

ABSTRACT

We evaluate the factors influencing the abundance, [Li], and isotopic composition of riverine Li delivered to the oceans through analyses and modeling of [Li] and δ^7Li in streams and groundwaters draining a single continental lithology, the Columbia River Basalts (CRBs). The streams were sampled in different climate zones that lie east (dry), and west (wet) of the Cascades Mountains, and during two different seasons (summer and late winter) in order to evaluate climatic and seasonal influences on Li isotopes in rivers. Dissolved Li ($\delta^7Li_{dis} = +9.3$ to $+30.4$) is systematically heavier than that of fresh or weathered CRBs (-4.7 to $+6.0$, Liu et al., 2013), suspended loads (-5.9 to -0.3), and shallow groundwaters ($+6.7$ to $+9.4$), consistent with previous studies showing that Li isotope fractionation is affected by equilibration between stream water and secondary minerals. However, the lack of correlation between δ^7Li_{dis} and climate zone, the uniform secondary minerals and bedrock, coupled with the highly variable (>20‰) δ^7Li_{dis} indicate that other factors exert a strong control on δ^7Li_{dis}. In particular, the heavier Li in streams compared to the shallow groundwaters that feed them indicates that continued isotopic fractionation between stream water and suspended and/or bed loads has a major influence on riverine δ^7Li. Seasonal δ^7Li variation is observed only for streams west of the Cascades, where the difference in precipitation rate between the dry and wet seasons is greatest. Reactive transport model simulations reveal that riverine δ^7Li is strongly controlled by subsurface residence times and the Li isotope fractionation occurring within rivers. The latter explains why there is no positive correlation between δ^7Li and traditional weathering proxies such as Si or normalized Si in rivers, as riverine Li isotope fractionation drives δ^7Li to higher values during transport, whereas the concentrations of major cations and anions are diluted. The varying residence time for groundwaters feeding the western streams in summer (long residence times, higher δ^7Li, greater weathering) and winter (short residence times, lower δ^7Li, less weathering) explains the observed seasonal variations. A global, negative correlation between δ^7Li and Li/Na for streams and rivers draining basaltic catchments reflects the overall transport time, hence the amount of silicate weathering. Based on our results, the increase of δ^7Li in seawater during the Cenozoic is unlikely related to changing climate, but may reflect mountain building giving rise to increased silicate weathering.

1. Introduction

Chemical weathering of silicate rocks on Earth's surface plays a critical role in regulating the global carbon cycle over geological time-scales (e.g., Berner et al., 1983). Basalt weathering, in particular, may significantly contribute to the global silicate weathering flux. For example, Gaillardet et al. (1999), suggested a minimum of 25% of the silicate weathering flux to the oceans derives from weathering of basalt. Attempts to illuminate chemical weathering processes using natural samples generally take two approaches: studies of river waters (e.g., Dessert et al., 2001; Gaillardet et al., 1999), and studies of weathering profiles or weathered regoliths (e.g., Brimhall et al., 1991; Nesbitt and Wilson, 1992). River chemistry is able to provide rate-related constraints, such as chemical weathering fluxes and CO_2 consumption rates (Gaillardet et al., 1999), although only for the present.

Li isotopes can potentially provide insights into the weathering flux from the continents over time (Liu and Rudnick, 2011), and changing climate, if the changes in δ^7Li in the seawater record (Misra and Froelich, 2012) can be deciphered. The Li isotopic

* Corresponding author at: Geophysical Lab, Carnegie Institute of Washington, 5251 Broad Branch Rd. NW, Washington, DC 20015-1305, USA. Tel.: +1 (301) 825 6841, fax: +1 (202) 478 8901.
E-mail address: xliu@gl.ciw.edu (X.-M. Liu).

http://dx.doi.org/10.1016/j.epsl.2014.10.032
0012-821X/

composition in seawater is a function of the input of rivers and hydrothermal fluid, and the output into secondary minerals formed via low temperature basalt alteration and sediment clay authigenesis (referred to as "reverse weathering") (Chan et al., 1992). The dramatic (8‰) increase in δ^7Li in seawater through the Cenozoic has been interpreted to reflect the changing composition of riverine inputs that, in turn, reflect climatic and tectonic influences on continental weathering (Misra and Froelich, 2012). Assuming a constant hydrothermal input, the significant increase in δ^7Li through the Cenozoic may indicate increases in the riverine input (a greater flux and/or higher δ^7Li), an increased output flux of low δ^7Li, or both. Therefore, understanding the controls on riverine Li isotopes is a first-order requirement for understanding the secular evolution of seawater.

Li is contained mainly in silicates and is released, with attendant isotopic fractionation, during weathering (e.g., Huh et al., 2001, 1998; Kisakürek et al., 2005, 2004; Rudnick et al., 2004). Lithium's two stable isotopes, ^{7}Li and ^{6}Li, have great fractionation potential due to their 17% mass difference. Differences in Li isotopic composition are expressed as $\delta^7\text{Li}\ (‰) = ([^7\text{Li}/^6\text{Li}]_{\text{sample}}/[^7\text{Li}/^6\text{Li}]_{\text{standard}} - 1) \times 1000$, where the standard used is a lithium carbonate, L-SVEC (Flesch et al., 1973). Lithium is a water-soluble trace element, but neither primary basalt dissolution nor metamorphic dehydration appear to cause significant Li isotopic fractionation (Marschall et al., 2007; Pistiner and Henderson, 2003; Qiu et al., 2011a, 2011b, 2009; Teng et al., 2007; Wimpenny et al., 2010a). By contrast, Li isotopes fractionate significantly during incongruent continental weathering, due to the formation of secondary minerals, such as clays (e.g., Huh et al., 1998; Kisakürek et al., 2004; Pistiner and Henderson, 2003; Pogge von Strandmann et al., 2006; Rudnick et al., 2004; Teng et al., 2004). Lithium has a few more advantages as a potential geochemical tracer of weathering. Li has only one redox state (+1 charge), and is thus insensitive to changes in oxygen fugacity compared to Fe, Cr, Cu, Mo, etc. In addition, Li is not a nutrient, so its elemental and isotopic behavior is not directly influenced by biological processes (e.g., Lemarchand et al., 2010). Finally, Li is enriched in silicates and depleted in carbonates, so its abundance and isotopic composition in rivers mainly reflect continental silicate weathering (one caveat is that riverine Li can be significantly influenced by the presence of evaporites, e.g., Huh et al., 1998).

Studies investigating the use of δ^7Li as a weathering proxy (Huh et al., 2001, 1998; Millot et al., 2010; Pogge von Strandmann et al., 2006; Vigier et al., 2009) have not fully discerned why the Li isotope composition of rivers does not show consistent correlation with certain silicate weathering proxies. For instance, Huh et al. (1998) did not observe a clear correlation between $\delta^7\text{Li}_{\text{dis}}$ and $^{87}\text{Sr}/^{86}\text{Sr}$, $\delta^7\text{Li}_{\text{dis}}$ and [Li] (using square brackets around elements to indicate concentration) as well as between $\delta^7\text{Li}_{\text{dis}}$ and Si/TZ^+ (Total cation charge, $\text{TZ}^+ = \text{Na}^+ + 2\text{Mg}^{2+} + \text{K}^+ + 2\text{Ca}^{2+}$ in 10^{-3} equivalents per liter, mEq/L) when compiling global river data. By contrast, for the Orinoco drainage basin a strong inverse correlation was observed between $\delta^7\text{Li}_{\text{dis}}$ and $^{87}\text{Sr}/^{86}\text{Sr}$ as well as between $\delta^7\text{Li}_{\text{dis}}$ and Si/TZ^+ (Huh et al., 2001). In addition, in some studies a correlation between δ^7Li and chemical weathering rates (in mass/area/time) was observed (Vigier et al., 2009), whereas in others no clear relationship could be identified (Millot et al., 2010). The lack of consistent correlation may reflect variations in climate (e.g., tropical vs. temperate climates), lithologies, hydrology, and sampling seasons encompassed in previous river studies. Here we seek to illuminate the causes of Li isotopic fractionation produced during weathering by studying surface waters draining a single lithology (basalt) as a function of climate, season, and groundwater residence time. The Columbia River Basalts (CRBs) afford this opportunity due to their large areal extent, which encompasses different climate zones and allows sampling within a single lithology having limited isotopic variability. Understanding the processes that control $\delta^7\text{Li}_{\text{dis}}$ will, in turn, afford greater insight into the changing δ^7Li observed in seawater with time.

2. Geological setting, climate and samples

The geological setting of the sampling area is described in Liu et al. (2013) and a brief account is provided here. The CRBs are continental flood basalts that erupted during the Miocene (between 17 Ma and 6 Ma) in the US Pacific Northwest, covering large parts of southern Washington, northeastern Oregon and parts of western Idaho (Fig. 1).

The CRBs crop out both east and west of the Cascade Mountain Range. The Cascades developed progressively from subduction zone magmatism since the Late Eocene, with topography increasing more or less steadily since the Late Oligocene (Kohn et al., 2002 and references therein). The mountains created two different climate zones that affected the CRBs via the rain shadow effect; regions west of the Cascades have high mean annual precipitation (MAP) (1500–2000 mm), whereas annual precipitation east of the Cascades is less than 300 mm (Kohn et al., 2002; Takeuchi et al., 2010). In addition, the monthly precipitation rates vary more in the west, where the mean monthly precipitation rate during the wet season (October–May) is up to 10 times greater than that during the dry season (June–September) (Fig. A1). By contrast, differences in monthly precipitation rates east of the Cascades are usually less than a factor of 2.

The advantages of studying streams and groundwaters in this area include: 1) The streams only drain a single lithology, the CRBs. 2) Sampling streams from different climate zones allows investigation of how annual precipitation rates, and thus climate, may have influenced riverine Li isotopic composition. 3) Due to the variable seasonal precipitation (Fig. A1), sampling in two seasons allow us to assess the effect of seasonally variable precipitation rates and corresponding variable surface runoff (Fig. A2) on Li isotopic compositions. 4) Sampling of groundwaters that are the potential sources of the streams allows distinction between Li isotope fractionation occurring in subsurfaces and fractionation occurring in rivers.

3. Samples and analytical methods

3.1. Sampling

Dissolved and suspended load samples from 10 CRB streams were collected in July 2010, and again in March 2012 to study possible seasonal variations; samples from the mouths of the much larger Deschutes and John Day rivers, which have lithologically diverse catchments, were also taken for comparison. In addition, five groundwater samples were collected in March 2012, as well as an additional stream (Mosquito Creek, R11) (Fig. 1).

At each site, pH, temperature, electrical conductivity, and total dissolved solids (TDS) were measured using a multi-meter (Hanna® Instruments) with analytical accuracy of ±0.05, ±0.5 °C, ±2% µS/cm, and ±2% ppm, respectively. All stream water samples were obtained using a peristaltic pump and filtered using a 142 mm filter holder system with 0.2 µm cellulose acetate filters. Filtered waters were collected in pre-cleaned Nalgene® bottles. Filters were placed in air-tight Ziploc plastic bags for transport back to the lab. The suspended loads of the stream waters were recovered from the filters in the clean lab. The sample tubing was pumped dry after each sample collection and one liter of deionized water was pumped through the system to clean it between each sampling event. At the start of sampling at a new site, a liter of sample water was first collected into the pre-cleaned bottles

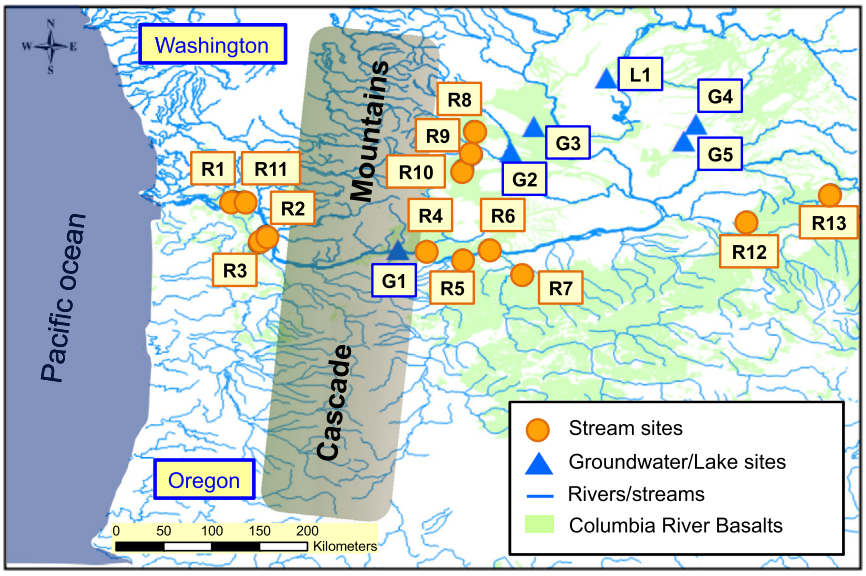

Fig. 1. Map of sample locations. Geological data are from USGS. Stream sample locations are shown in orange circles and numbered with Rx. R11 was only sampled during late winter of 2012 and the rest rivers were sampled both in summer of 2010 and late winter of 2012. Groundwater sample locations and one lake sample location are shown in blue triangles, all of which were sampled during late winter. (For interpretation of the references to color in this figure legend, the reader is referred to the web version of this article.)

and then discarded. Finally, about two liters of water were collected, acidified using five drops (~0.25 ml) of concentrated HCl and stored in Nalgene® bottles for transport to the lab. Following this procedure, two 125 ml pre-cleaned Nalgene® bottles were filled with water for anion (without acidification) and major and trace cation analyses (acidified using two drops of ~0.1 ml concentrated HCl).

Groundwaters were sampled either from existing pumping systems that tap into deep-seated subsurfaces or faucets fed by shallow wells. The sampling method outlined above for streams was also used for the groundwaters (Table 2). One groundwater sample (G4, Lind) was taken from a new municipal well in the town of Lind, WA, which taps into a subsurface buried 220 m below ground and is estimated to be >50 ka old based on radiocarbon age dating (T. Tolan, personal communication). A second groundwater sample (G1, Spring Creek) was collected at the Spring Creek National Fish Hatchery from a subsurface ~200 m deep, containing little or no modern water and having an overall age of thousands of years (Hinkle, 1996). Thus, these two groundwaters are unlikely to be the sources of waters in the streams.

3.2. Major and trace elements in dissolved loads

Major and trace cations in dissolved loads were analyzed using an Element 2 single collector Inductively Coupled Plasma-Mass Spectrometer (ICP-MS) at the University of Maryland. Calibration curves were created using pure element solutions (Alfa Aesar®) and standard and water samples were doped with the same amount of indium to correct for instrumental drift ([In] = 2 ppb). The accuracy and precision of the analyses were determined by repeat analyses of the international river standard SLRS-5, with accuracy of cations assessed at better than 4% ($n = 11$ for SLRS-5), except for K (<10%), based on its certified value (Table A.1).

Major anion concentrations were measured by ion chromatography in the Biogeochemical Lab at the University of Maryland. Anion concentrations were measured using a Dionex ICS-1500 ion chromatograph, equipped with an AS14 4-mm analytical column and a guard column. An eluent of 3.5 mM of Na_2CO_3 with 1.0 mM $NaHCO_3$ was used at a flow rate of 0.3 mL/min. The detection limits of the ion chromatograph are 0.01 mg/L, 0.01 mg NO_3/L and 0.02 mg SO_4/L for Cl^-, NO_3^- and SO_4^{2-}, respectively. The accuracy of the analyses are better than ~5% based on repeat analyses of standards (see Table A.2). HCO_3^- concentrations were estimated based on charge balance.

3.3. Lithium isotope analyses

All sample preparation and analyses were performed in the Geochemical Laboratory at the University of Maryland. A description of sample dissolution, column chemistry, analytical blanks and instrumental analysis is provided in the electronic appendix (Text A1). Long-term precision is better than ±1‰ (2σ); several USGS rock standards were run repeatedly during the course of this study (Table A.3). BHVO-1 yielded δ^7Li of $+4.6 \pm 1.0$ ($n = 5$) cf. 4.0 to 5.6 in the literature (GeoReM database: http://georem.mpch-mainz.gwdg.de/); BCR-2 yielded δ^7Li of $+2.9 \pm 1.5$ ($n = 3$) cf. 2.6 to 4.6 in the literature (GeoReM database); and AGV-1 yielded δ^7Li of $+5.2 \pm 0.6$ ($n = 3$) cf. 4.6 and 6.7 for AGV-1 in Liu et al. (2010) and Magna et al. (2004), respectively.

3.3.1. Handling of dissolved loads

Approximately 30 ml to 2 L of filtered stream and groundwaters (depending on the volume collected) were first weighed and then evaporated in large Savillex® Teflon beakers (160 ml) or Teflon evaporation dishes (400 ml) on a hot plate ($T < 100\,^\circ$C). A 3:1 mixture of HF–HNO_3 was added to the samples, which were then transferred into screw-top Savillex® Teflon beakers (15 ml) placed onto a hot plate ($T < 120\,^\circ$C) for an overnight dissolution followed by an evaporation step. The sample was then treated with concentrated HNO_3 and HCl until all solids were dissolved and the final solutions were clear. The final dried sample was picked up in 4 N HCl for column separation.

3.3.2. Dissolution of suspended loads

Suspended load samples were washed off the filters into large Savillex® Teflon beakers (160 ml) using Milli-Q water and then transferred into screw-top Teflon beakers and dried on a hot plate ($T < 70\,^\circ$C). The dried samples were then scraped off the beaker and weighed into clean Teflon beakers; sample sizes ranged from several milligrams to tens of milligrams. The samples were then dissolved using a 3:1 mixture of HF and HNO_3 in a screw-top

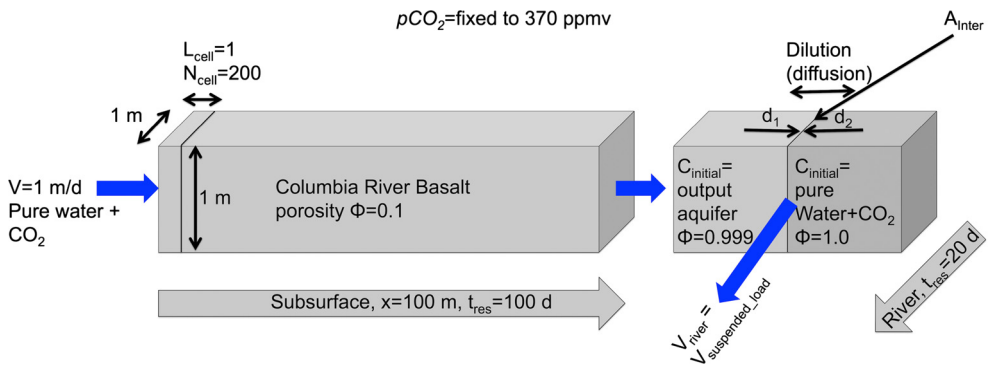

Fig. 2. Model setup illustrating that simulations were run for a 100 m long subsurface that eventually exfiltrates into a river. River simulations were run as batch simulations (no flow) assuming that the suspended load is transported at the same velocity as river water. Moreover, river simulations consider a diffusive dilution of the exfiltrated groundwater with water that experienced no previous water–rock interaction (i.e., pure water+CO_2). For both systems (subsurface and river), Li isotope fractionation is simulated to occur during hematite and kaolinite precipitation.

Teflon beaker on a hot plate ($T \approx 90\,^{\circ}C$), dried, then pickup up by HNO_3 and HCl addition until all solids were dissolved and the final solutions were clear. The final dried sample was dissolved in 4 N HCl for column separation.

3.4. Reactive transport modeling

In order to investigate the influence of silicate weathering on δ^7Li_{dis}, a series of thermodynamically- and kinetically-controlled reactive transport model simulations were carried out using the code TOUGHREACT V2 (Xu et al., 2011). TOUGHREACT has been used to evaluate isotopic fractionation coupled to water–rock interaction and hydrological processes in a variety of subsurface environments and laboratory experiments (e.g., Singleton et al., 2005; Sonnenthal et al., 1998; Wanner and Sonnenthal, 2013). Each modeled scenario is composed of two individual simulations to model silicate weathering and associated Li isotope fractionation (i) during subsurface flow and (ii) within rivers (Fig. 2). The model setup is closely related to the simulations performed by Wanner et al. (2014) modeling Li isotope fractionation associated with granite weathering. Accordingly, only a short model description is provided below. Input parameters and specific code capabilities used to simulate Li isotope fractionations are described in detail in the electronic appendix (Text A2).

3.4.1. Subsurface simulations

Reactive transport along a basaltic subsurface was simulated for a fully saturated, 100 m long porous media having a porosity of 10%, the porosity previously used to simulate Columbia River Basalt weathering (Taylor and Lasaga, 1999). Fracture flow, the presence of highly porous flow tops, as well as the unsaturated zone, were not incorporated into the model because our focus is on assessing the sensitivity (i.e., trends) of dissolved δ^7Li values as a function of residence time (i.e., amount of weathering), rather than on simulating detailed flow features of actual unsaturated zones feeding subsurfaces and streams. Subsurface simulations were run for an average linear groundwater flow velocity of 1 m/d to simulate a system dominated by advection.

Pure water in equilibrium with atmospheric CO_2 was specified as the initial and boundary fluid compositions. A starting mineralogical composition similar to the normative mineralogy reported for different Columbia River Basalt members (BVSP, 1981) (e.g., plagioclase, pyroxene, olivine, glass) was assigned to the solid part of the porous medium (see Tables A.4 and A.5 for mineral stoichiometries, corresponding thermodynamic and kinetic parameters and specified initial and boundary conditions). Simulations were run for two different initial bulk Li concentrations of 4 and 20 ppm, encompassing most of the range of [Li] observed in fresh CRB (Liu et al., 2013), and to assess whether the initial Li concentration influences riverine δ^7Li values.

Because Li is moderately incompatible during igneous differentiation (Brenan et al., 1998), Li is assumed to be mostly contained within a glassy basalt matrix and is introduced into the model from a Li-bearing volcanic glass phase tabulated in the THERMODEM database (Blanc et al., 2012). Li-bearing hematite and kaolinite were allowed to precipitate. It should be noted that kaolinite and hematite are likely not the only secondary minerals forming, but they serve as representatives for any other potentially precipitating Fe- and Al-bearing minerals.

To simulate the fate of individual Li isotopes, ^6Li and ^7Li were incorporated into the mineral stoichiometries of primary Li-bearing volcanic glass, and secondary kaolinite and hematite. An initial δ^7Li value of $+1$ was assumed for Li-bearing glass, which corresponds to the average δ^7Li value measured for two different CRBs members (Liu et al., 2013). Similar to the model of Bouchez et al. (2013), we do not distinguish between Li exchange-, Li surface complexation-, or Li substitution reactions and Li uptake by secondary minerals and associated Li isotopic fractionation is solely simulated during Li incorporation into precipitating kaolinite and hematite. Li bearing secondary mineral precipitation is simulated by means of a solid solution approach, such as described in detail by Wanner et al. (2014), as well as in Text A2. A fractionation factor ($\Delta^7Li_{2ndMin\text{-}solution} = \delta^7Li_{2ndMin} - \delta^7Li_{solution}$) of $-10‰$ was assigned for hematite and kaolinite precipitation, which is within the range of Li isotope fractionation factors reported or inferred for secondary mineral precipitation (Huh et al., 2001; Kisakürek et al., 2005; Pistiner and Henderson, 2003; Pogge von Strandmann et al., 2006, 2010; Vigier et al., 2009; Zhang et al., 1998). An extended discussion of fractionation factors can be found in Text A2.

3.4.2. River simulations

River simulations were conducted essentially as batch simulations, where the flow velocity was set to zero. In doing so, it was assumed that the reactive suspended load (i.e., solid phase) is transported at the same velocity as the river water, which is in agreement with current knowledge about the transport of suspended river loads (Fryirs and Brierley, 2013).

Two grid blocks were defined to simulate groundwater exfiltrating into river systems, which is diluted by river water that previously experienced less water–rock interaction processes. By setting the interfacial area (A_{inter}, Fig. 2) between the two grid blocks to 7000 m^2, the Li concentration of the exfiltrating groundwater was diluted by a factor of $\sim$10 during a simulated river residence time of 20 days, roughly corresponding to the Li concentration difference observed between streams and groundwaters (Tables 1, 2).

Table 1
Sample locations, field measurements, major and trace element concentrations and Li isotopic compositions in dissolved and suspended loads of rivers.

2010 summer	Units	Cameron	Milton	N. Scapoose	Silva	Deschutes	John Day	Hay	Wenas	Cowiche	Ahtanum	Mill	Asotin
Sample #		R1	R2	R3	R4	R5	R6	R7	R8	R9	R10	R12	R13
Longitude	°	−123.16707	−122.84415	−122.91550	−121.26745	−120.90903	−120.65085	−120.31797	−120.79715	−120.82127	−120.90663	−118.11638	−117.29242
Latitude	°	46.20735	45.86973	45.79293	45.71217	45.63033	45.72850	45.47992	46.89620	46.66437	46.51642	46.00358	46.27363
Location[a]		west	west	west	east	east	east	east	east	east	east	east	east
T	°C	15.6	18.6	15.2	18.1	19.2	21.9	19.6	12.6	18.8	14.6	14.1	18.1
pH		7.2	7.7	7.9	8.0	8.7	8.5	7.8	7.9	8.0	7.8	7.8	8.1
Conductivity	μS/cm	21	64	65	130	120	160	310	95	88	65	74	82
TDS	mg/L	10	32	32	64	58	82	150	47	44	32	35	41
Na	mg/L	2.7	4.9	5.3	6.5	9.6	7.0	17	3.9	4.0	3.2	3.8	3.5
Mg	mg/L	0.8	2.1	1.9	5.4	4.7	5.9	11	4.5	3.8	2.7	2.5	3.1
Al	μg/L	30	12	22	6.5	6.1	4.7	1.8	9.1	15	10	6.5	20
Si	mg/L	6.5	17	22	31	20	14	41	29	32	27	29	30
K	mg/L	0.4	1.1	1.3	1.5	1.7	1.4	3.7	1.6	2.1	1.8	2.3	2.3
Ca	mg/L	1.7	4.9	5.2	11	6.8	16	28	8.9	7.9	6.3	6.6	8.0
Fe	μg/L	130	320	170	28	21	32	54	130	180	79	50	35
F^-	mg/L	0.06	0.08	0.04	0.56	–	0.13	0.13	0.04	0.06	0.03	0.07	0.08
Cl^-	mg/L	2.6	4.0	18	54	13	8.5	8.6	16	13	16	3.2	2.8
NO_3^-	mg/L	–	–	–	–	–	–	0.01	–	–	0.01	–	–
SO_4^{2-}	mg/L	2.1	4.7	5.5	39	1.3	4.3	18	2.7	1.4	5.1	3.4	1.9
HCO_3^-	mg/L	0.9	0.9	1.3	1.0	1.5	2.7	−0.4	0.6	1.1	0.9	0.9	1.5
Li_{dis}	μg/L	0.1	0.7	1.6	0.4	4.7	1.6	3.2	0.7	1.1	0.7	0.9	1.0
δ^7Li_{dis}		21.1	22.1	14.9	30.4	12.2	16.6	20.0	20.2	17.0	13.0	10.6	9.3
Li_{sus}	μg/g	–	–	14	–	7.5	15	–	24	–	–	–	7.2
δ^7Li_{sus}		–	–	−5.6	–	4.2	−1.6	–	-3.1	–	–	–	−4.2

2012 winter	Units	Cameron	Milton	N. Scapoose	Silva	Deschutes	John Day	Hay	Wenas	Cowiche	Ahtanum	Mill	Asotin	Mosquito
Sample #		R1	R2	R3	R4	R5	R6	R7	R8	R9	R10	R12	R13	R11
Longitude	°	−123.16707	−122.84415	−122.91550	−121.26745	−120.90903	−120.65085	−120.31797	−120.79715	−120.82127	−120.90663	−118.11638	−117.29242	−123.06510
Latitude	°	46.20735	45.86973	45.79293	45.71217	45.63033	45.72850	45.47992	46.89620	46.66437	46.51642	46.00358	46.27363	46.20202
Location[a]		west	west	west	east	east	east	east	east	east	east	east	east	west
T	°C	5.8	6.0	5.2	5.6	8.0	6.9	9.0	1.4	2.2	2.9	4.3	5.2	5.6
pH		6.7	6.9	8.3	7.6	8.0	7.7	7.8	7.6	7.6	7.6	7.4	7.6	6.7
Conductivity	μS/cm	14	31	37	65	110	130	320	97	100	91	51	74	20
TDS	mg/L	7	16	18	33	52	62	160	48	51	44	25	37	10
Na	mg/L	2.2	3.1	3.2	4.2	8.2	5.6	16	4.0	4.6	3.9	3.1	2.9	2.4
Mg	mg/L	0.6	1.0	1.0	2.7	4.0	4.4	10	4.3	4.4	3.6	1.7	2.7	0.8
Al	μg/L	16	4.9	8.9	86	43	40	2.1	57	23	22	180	240	12
Si	mg/L	4.1	9.2	12	21	22	19	34	27	30	30	24	27	4.8
K	mg/L	0.3	0.6	0.8	0.9	1.5	1.3	3.8	1.5	1.9	2.0	1.5	1.7	0.3
Ca	mg/L	1.6	2.8	3.1	6.3	6.4	12	27	8.6	8.8	7.9	4.8	6.9	1.9
Fe	μg/L	20	14	16	55	34	51	57	93	76	55	220	250	37
F^-	mg/L	0.01	0.02	0.03	0.04	0.10	0.08	0.42	0.09	0.10	0.07	0.15	0.08	0.01
Cl^-	mg/L	3.3	2.6	2.9	1.6	1.8	1.2	11	0.4	0.9	0.4	0.5	0.7	2.7
NO_3^-	mg/L	2.0	3.3	2.8	0.0	0.4	0.3	1.5	0.0	0.0	0.0	0.2	0.3	4.8
SO_4^{2-}	mg/L	0.5	1.2	1.6	0.7	1.8	3.9	15	2.0	3.2	1.6	0.6	1.3	0.5
HCO_3^-	mg/L	0.6	0.4	0.7	2.5	2.6	2.6	3.9	1.7	1.8	3.1	7.2	9.6	0.6
Li_{dis}	μg/L	0.1	0.4	0.9	0.3	3.5	1.1	2.9	0.5	1.1	0.8	0.7	0.7	0.2
δ^7Li_{dis}		17.4	13.0	8.8	14.0	12.5	13.5	18.8	21.6	16.1	13.1	10.9	8.9	15.9
Li_{sus}	μg/g	16	20	66	18	13	20	21	24	16	16	19	36	17
δ^7Li_{sus}		−1.4	−2.5	−4.5	−0.9	−0.3	−1.5	−0.2	−3.1	−5.7	−5.9	−2.8	−5.2	−1.0

[a] Location relative to the Cascades (west or east).
Note: "–" Under detection limit.

Table 2
Sample locations, field measurements, major and trace element concentrations and Li isotopic compositions of groundwaters and one alkaline lake.

Groundwater	Units	Spring Creek	Selah	Ryegrass	Lind	Hatton	Soap Lake
Sample #		G1	G2	G3	G4	G5	L1
Longitude	°	−121.54613	−120.44327	−120.20900	−118.62250	−118.74282	−119.49877
Latitude	°	45.72737	46.69758	46.94738	46.96828	46.79410	47.42263
Sampling[a]		well	faucet	faucet	well	faucet	
T	°C	17.6	18.1	14.7	28.6	10.9	10.2
pH		8.8	8.0	7.7	9.1	7.9	9.6
Conductivity	µS/cm	180	320	340	350	510	>3999
TDS	mg/L	90	160	170	180	250	> 2000
Na	mg/L	33	21	13	78	19	280
Mg	mg/L	0.4	12	15	0.3	19	4.4
Al	µg/L	6.9	27	0.5	4.9	0.1	–
Si	mg/L	45	33	40	64	35	4.9
K	mg/L	4.5	3.9	2.9	3.9	4.0	590
Ca	mg/L	1.9	17	19	3.1	40	6.9
Fe	µg/L	47	6.9	5.7	17	54	1.3
F^-	mg/L	0.76	0.48	0.39	3.3	0.28	0.31
Cl^-	mg/L	3.6	8.6	7.0	7.9	46	130
NO_3^-	mg/L	0.01	–	11	0.1	18	–
SO_4^{2-}	mg/L	1.5	3.7	12	4.7	50	210
HCO_3^-	mg/L	3.5	1.8	2.4	2.4	3.4	−0.87
Li_{dis}	µg/L	21	9.8	6.5	8.9	3.3	1.5
δ^7Li_{dis}		6.8	8.1	9.4	21.4	6.7	20.5

[a] Sampling methods (well or faucet).
Note: "–" Below detection limit.

Reactions between the suspended river load and river waters were only considered for the grid block initially containing exfiltrating groundwater.

The suspended river load was assigned the same initial mineralogical composition as the subsurface (Table A.5), assuming that this load contains a significant amount of primary silicate minerals in addition to the dominant clays and oxides (Gaillardet et al., 1999). This model assumption is consistent with Bouchez et al. (2011) who observed that the mineralogical composition of the suspended load is dependent on the particle size and that primary silicate minerals (e.g., feldspar) are enriched in the coarser fraction. Consequently, Li isotope fractionation in the simulated river is assumed to occur in the same fashion as in the subsurface simulations.

4. Results

Data for field measurements (pH, temperature, electrical conductivity, and TDS), major and trace elements, in addition to Li isotopic data are given in Tables 1 and 2, for streams and groundwaters, respectively. A comparison between summer and late winter data is shown in Figs. A3 and A4 for field parameters and selected dissolved species, respectively.

4.1. Field measurements

Streams sampled in July 2010 display a temperature range from 13 to 22 °C with pH ranging from 7.2 to 8.7, while the streams sampled in March 2012 are cooler (1 to 9 °C), but have a similar range in pH (6.7 to 8.3). Groundwaters are warmer (10 to 29 °C), and have higher pH (7.7 to 9.6), compared to the streams sampled at the same time of the year (March). TDS in streams east of the Cascades do not show significant seasonal variations (32 to 154 mg/L in July, and 25 to 158 mg/L in March, Table 1) with the exception of Silva creek, where TDS varies by a factor of two between seasons (64 in summer vs. 33 ppm in winter). By contrast, TDS in the three streams west of the Cascades differ by up to a factor two between seasons (7–18 mg/L in July, 10–32 mg/L in March). Groundwaters range to higher TDS values (90 to 253 mg/L, Table 2). The maximum TDS value was measured in a meromictic lake (i.e., a stratified lake that does not mix between layers), the TDS of which exceeded the range of the multi-meter.

4.2. Major elements

Major cations and anions in stream water and groundwater samples are plotted using a classic Piper Diagram (Piper, 1953), a trilinear diagram consisting of two equilateral triangles for cations and anions, respectively, which are projected onto a central diamond (Fig. 3). In the lower triangles, the points are expressed as a percentage of the total amount of cations or anions in milliequivalents per liter. River and groundwaters are plotted in Figs. 3a and 3b for summer and winter, respectively. River waters have clustered cation patterns in both summer and winter illustrating that the water chemistry is inherited from a single lithology. Three shallow groundwaters plot within the same domain as the streams, while two deep groundwaters (G1: Spring Creek, and G4: Lind) show very different cation and anion patterns. Major elements such as Na, Si and Ca, correlate with Mg, and hence with each other (Fig. A5). Similarly, the total cation charge, TZ^+ ($TZ^+ = Na^+ + 2Mg^{2+} + K^+ + 2Ca^{2+}$ in 10^{-3} equivalents per liter, mEq/L), also correlates ($R^2 = 0.98$) with [Mg] in stream waters. Groundwaters, except for the two deep groundwaters (G1: Spring Creek, and G4: Lind), follow the same major element correlation, but with higher concentrations. The sample from Silva Creek taken in July, 2010, has much higher [Cl^-] (54 mg/L) and [SO_4^{2-}] (39 mg/L), compared to the other streams studied here and natural streams elsewhere (where [Cl^-] and [SO_4^{2-}] are typically less than 10 mg/L), indicating that this creek may have been subjected to anthropogenic contamination in the summer months (e.g., fertilizers).

Major cations in streams show very little variation between summer and winter; however, anions show large variations (Fig. 3). Although little variation is observed for cation ratios, actual concentrations (e.g., Si, Mg, and Na) tend to be slightly higher during the summer sampling campaign (Table 1, Fig. A4). This observation corresponds well with pH values and TDS concentrations, which were also slightly larger during the summer sampling campaign (Table 1, Fig. A3). In the case of [Si] and TDS, the seasonal concentration increase is most prominent in the western streams, with an increase of up to a factor two. By contrast, in the eastern streams both concentration variations ([Si] and TDS) were significantly smaller, by a factor less than ∼1.3 (Table 1). In addition, although there is some seasonal variation of anion concentrations

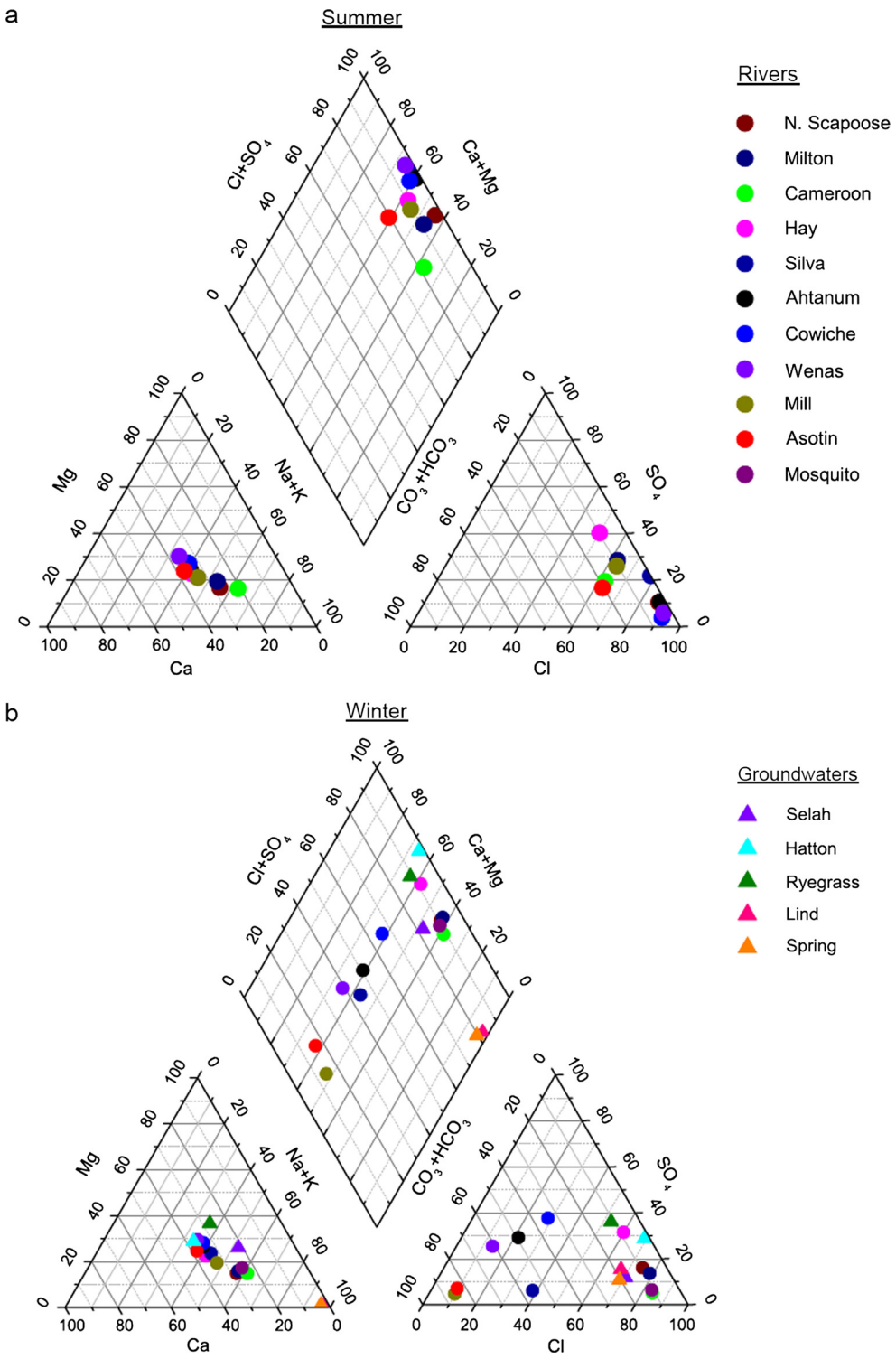

Fig. 3. Piper diagram (Piper, 1953) of streams and groundwaters in summer (a) and late winter (b). Stream waters and groundwaters are shown in circles and triangles, respectively. (For interpretation of the colors in this figure, the reader is referred to the web version of this article.)

among streams, the overall pattern likely reflects a mixture of water sources, since all streams and shallow groundwaters plot along a straight line; the two deep groundwaters fall off the trend in the upper diamond plot (Fig. 3).

4.3. Li elemental and isotopic data

The Li concentrations of dissolved loads vary from 0.2 to 4.7 μg/L for both sampling seasons. For individual streams, there is little difference in [Li] between the two sampling campaigns (Table 1, Fig. 4), where [Li] shows a weak positive correlation with [Mg] ($R^2 = 0.7$) and [Si] ($R^2 = 0.4$). δ^7Li_{dis} ranges from +10 to +30 in the streams sampled during the summer, and shows a similar range in the streams sampled in the late winter (+9 to +22). In streams east of the Cascades, δ^7Li_{dis} does not change with season, except for Silva Creek (+30 vs. +14‰), which may reflect anthropogenic contamination, based on the high contents of [Cl^-] and [SO_4^{2-}]. A previous study has shown that anthropogeni-

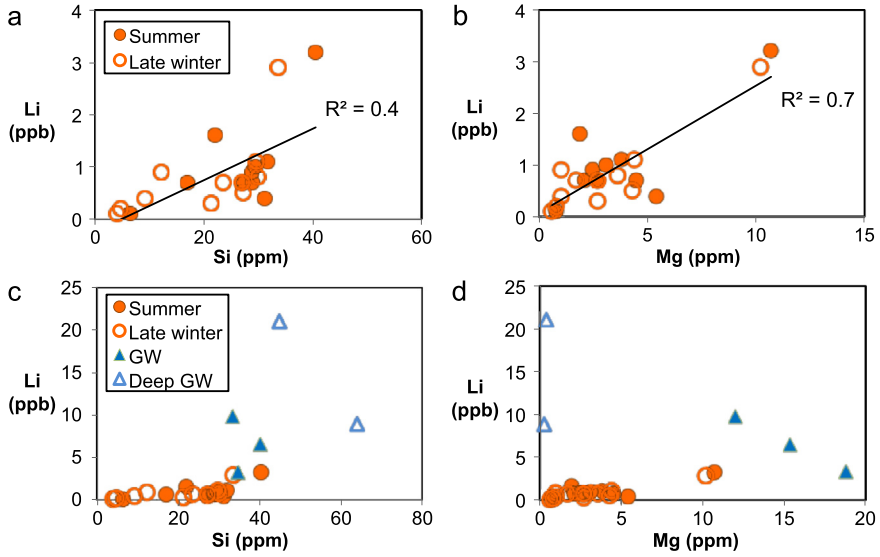

Fig. 4. Plots of [Li] versus [Si] and [Mg] in streams and groundwaters. Summer and late winter stream waters are shown in open and closed orange circles, respectively. Groundwaters feeding the streams are in solid blue triangles, deep seated and ancient groundwaters are shown in open blue symbols. (For interpretation of the references to color in this figure legend, the reader is referred to the web version of this article.)

cally contaminated groundwaters may show very heavy δ^7Li values (up to ~+1000‰), due to the use of heavy Li-enriched fertilizer (Négrel et al., 2010). By contrast, the streams to the west of the Cascades show consistently higher δ^7Li values in the summer compared to the winter (Fig. 5).

Varying from 2 to 21 μg/L (Table 1), groundwater [Li] is significantly higher than in the streams. Moreover, with the exception of the two groundwaters from deep wells (shown as open triangles in the figures), [Li] in groundwaters show similar correlations with [Si], but not with [Mg], as seen in stream waters (Fig. 4). Except for the deep-seated Lind well water (G4, +21.4‰), groundwater δ^7Li (δ^7Li_{GW}) are between +6.7 and +9.4‰, which is on the very low end of observed δ^7Li_{dis} (Tables 1, 2).

[Li] in the suspended loads varies from 7 to 24 μg/g in the streams sampled during the summer, and shows a greater range in the streams sampled during the late winter (from 13 to 66 μg/g). The δ^7Li of the suspended load (δ^7Li_{sus}) is generally the same from season to season, except for the Dechutes River, which shows a large change in δ^7Li_{sus} according to season (from +4.2 in summer to −0.3 in late winter). With the exception of the summer Deschutes River sample, δ^7Li_{sus} are lower compared to the average δ^7Li measured in fresh CRBs ($\delta^7Li = 1.1$, Liu et al., 2013). The low δ^7Li_{sus} are comparable to the lower than average δ^7Li observed in weathered CRB ($\delta^7Li = -5$ to 0) and the upper continental crust ($\delta^7Li = 0$ on average, Teng et al., 2004).

4.4. Simulation results

4.4.1. [Li] and δ^7Li

Simulated steady-state [Li] and [Si] profiles along our model domain (subsurface + river), as well as corresponding δ^7Li profiles (i.e., δ^7Li_{dis}, δ^7Li_{2ndMin} and $\delta^7Li_{bulk\text{-}rock}$) are shown in Figs. 6a and 6b for two different parental basalt Li concentrations of 4 and 20 ppm. Increasing [Li] in basalt yields larger dissolved Li concentrations for a specific subsurface residence time (Fig. 6a), but does not change δ^7Li values, as illustrated by superimposing δ^7Li_{dis} vs. residence time behavior (Fig. 6b). These results thus imply that subsurface and riverine δ^7Li values are not sensitive to the Li concentrations of the parent rock, nor to the subsequent variable riverine [Li]. This simulation result is supported by a lack of correlation observed between δ^7Li_{dis} and [Li] (Table 1).

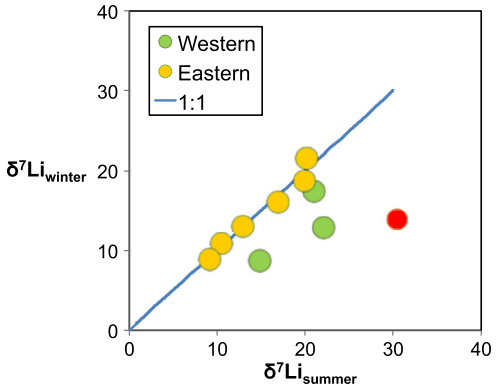

Fig. 5. Figure δ^7Li_{dis} in summer vs. winter for western and eastern streams. The sample showing suspected anthropogenic contamination (Silva, eastern) is plotted as a red circle (see main text for details). (For interpretation of the references to color in this figure legend, the reader is referred to the web version of this article.)

The δ^7Li_{dis} and δ^7Li_{2ndMin} values steadily increase with increasing subsurface and/or riverine residence time in the model (Fig. 6b). The slope of the δ^7Li increase with time is dependent on the specified fractionation factor. For a lower fractionation factor (i.e., less fractionation), longer residence time is needed to reach the same δ^7Li as for $\Delta^7Li = -10$‰, or vice versa. However, the pattern of increasing δ^7Li with increasing residence time is not sensitive to the specified fractionation factor. The δ^7Li_{dis} increases seen along the model domain are produced by our solid solution approach (Wanner et al., 2014), ensuring that [Li] in precipitating hematite and kaolinite increases with increasing [Li]. This assumption is consistent with an experimental study showing that [Li] in synthesized smectite increases linearly with aqueous [Li] (Decarreau et al., 2012). Because the dissolution rate of the parent rock remains constant (Table A.4), the ratio between Li that is incorporated into hematite and kaolinite, and the Li being released from the parent rock increases with increasing residence time, thus, continuously driving δ^7Li_{dis} and δ^7Li_{2ndMin} to higher values. The Li isotopic composition of the bulk rock is not changed (Fig. 6b) because the amount of secondary minerals formed during the 100 years for which the simulation were run were to low to drive the bulk rock δ^7Li to lower values. In contrast to δ^7Li_{dis} and

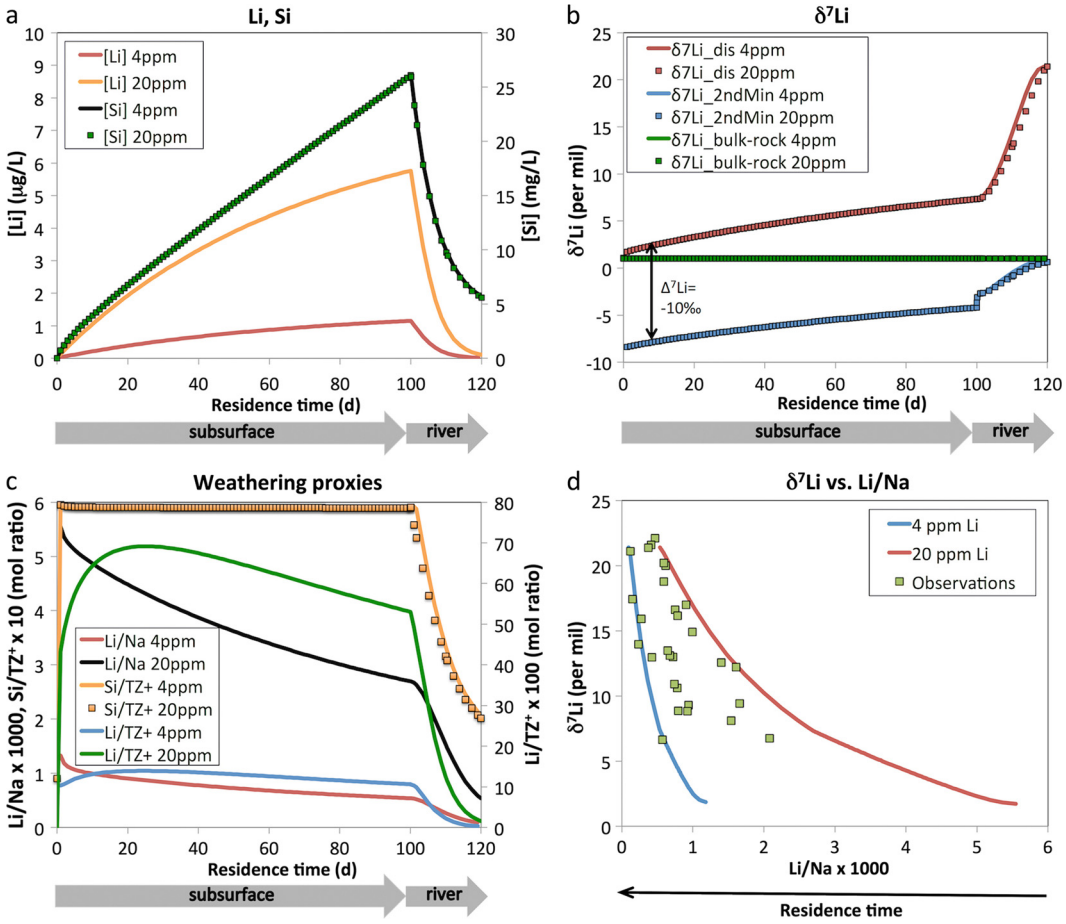

Fig. 6. Model results for initial CRB Li concentrations of 4 ppm and 20 ppm. (a) Illustrates steady state Li and Si concentration profiles along the full model domain (subsurface + river). (b) Presents corresponding steady-state δ^7Li profiles for aqueous Li (δ^7Li_{dis}), Li in precipitating secondary clays ($\delta^7Li_{kaolinite} = \delta^7Li_{hematite}$ summarized as δ^7Li_{2ndMin}) and Li of the bulk solid. (c) illustrates steady state profiles of typical silicate weathering tracers such as Si/TZ$^+$, Li/TZ$^+$ and Li/Na. (d) Comparison between the simulated δ^7Li vs. Li/Na relation (curves) and the one observed in groundwaters and streams draining the Columbia River Basalt (Tables 1 and 2). Decreasing Li/Na ratio reflects increasing subsurface and/or river residence time. All profiles are plotted against fluid residence time to simultaneously illustrate subsurface and river simulations. In the subsurface domain, fluid residence time (x-axis) also corresponds to the distance along the subsurface domain because the flow velocity was 1 m/d.

δ^7Li_{2ndMin}, aqueous [Li] and [Si] decrease (Fig. 6a) due to dilution when water flowing along the subsurface exfiltrates into the river.

4.4.2. Weathering proxies

Simulated profiles for silicate weathering proxies such as [Si], normalized Si (Si/TZ$^+$), [Li], normalized Li (Li/TZ$^+$), and Li/Na that have been previously used to constrain silicate weathering intensity (e.g., Huh et al., 2001, 1998; Millot et al., 2010; Pogge von Strandmann et al., 2010, 2006) are shown in Fig. 6c. These profiles reflect a proxy's ideal behavior, because processes potentially affecting the use of a specific weathering proxy (e.g., biological activity, anthropogenic contamination, salt leaching) were not considered in our simulations.

A negative correlation between δ^7Li_{dis} and Li/Na (Fig. 6c) reflects Li incorporation into hematite and kaolinite, whereas Na remains in solution. Accordingly, although [Li] also increases with residence time in the subsurface, the Li/Na ratio's decrease with increasing residence time is due to Li incorporation into these secondary minerals. Other weathering proxies show a distinct correlation with δ^7Li_{dis} only within a specific model domain (subsurface vs. river). In particular, concentration proxies such as [Si] and [Li] are positively correlated with δ^7Li_{dis} along the subsurface domain, but once exfiltrated, the correlations change sign because Li isotope fractionation is ongoing, whereas aqueous species concentrations decrease due to mixing with more superficial (i.e., meteoric) water.

5. Discussion

The observation that riverine δ^7Li_{dis} (+9 to +30) is systematically higher than δ^7Li values of the corresponding suspended loads ($\delta^7Li_{sus} = -6$ to 0), as well as fresh and weathered CRBs (δ^7Li = −5 to +5, Liu et al., 2013), confirms that high δ^7Li_{dis} is mainly generated by Li isotope fractionation occurring during basalt weathering (e.g., Huh et al., 2001, 1998; Pogge von Strandmann et al., 2010, 2006).

The most striking observation from our measurements, however, is the large variation in δ^7Li_{dis} (about 20‰ in summer, and >10‰ in late winter) covering almost the entire range of δ^7Li (+6 to +32) reported in major world rivers (Huh et al., 1998). This observation is especially remarkable because we sampled only small streams and groundwaters within the CRBs, for which catchment lithological differences are small. Some previous studies attribute large δ^7Li_{dis} variations to formation of different secondary minerals that have different fractionation factors with water (Millot et al., 2010; Wimpenny et al., 2010b). However, we see no evidence that the large δ^7Li_{dis} variations in our study are due to the presence of different Li-bearing secondary minerals, as saturation index (SI) calculations (Fig. A7) and studies of weathering profiles (Liu et al., 2013) suggest that all of the streams and groundwaters are saturated with the same secondary mineral assemblage (hematite, kaolinite and gibbsite). We therefore postulate that factors other than mineralogical differences (i.e., primary and

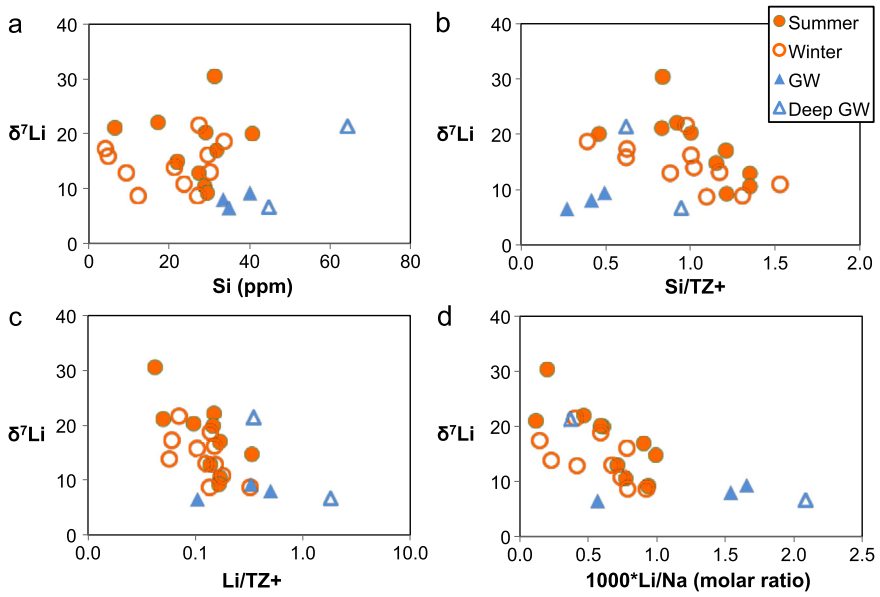

Fig. 7. δ^7Li_{dis} versus [Si], Si/TZ^+, Li/TZ^+, and $1000\times Li/Na$ (molar ratio) in stream waters and groundwaters. Summer and late winter stream waters are shown in open and closed orange circles, respectively. Groundwaters feeding streams are in solid blue triangles, deep-seated groundwaters are in open blue triangles. The total cation charge (TZ^+) is defined as $TZ^+ = Na^+ + 2Mg^{2+} + K^+ + 2Ca^{2+}$ in 10^{-3} equivalents per liter, mEq/L. (For interpretation of the references to color in this figure legend, the reader is referred to the web version of this article.)

secondary Li bearing phases) have a major control on the Li isotopic composition of the streams.

5.1. Residence time

The rise of δ^7Li with increasing residence time seen in the simulation (Fig. 6b) implies that subsurface residence time in particular, and the hydrological cycle in general have major controls on δ^7Li_{dis}. In fact, in a plot of δ^7Li_{dis} vs. Li/Na, our sample observations fall between the two curves defined by the minimum and maximum simulated bulk rock [Li] (Fig. 6d). We infer that the Li/Na ratio is an excellent proxy for residence time, because [Na] is at least three orders of magnitude higher than [Li] (Tables 1 and 2) and thus is not as strongly affected by small amounts of secondary mineral precipitation. However, Li/Na is also affected by the bulk rock concentration and the slope of the δ^7Li_{dis} vs. Li/Na correlation seems to be a function of the bulk rock [Li], whereas the location along a particular correlation (i.e., the measured δ^7Li_{dis} value) defines the residence time (Fig. 6d).

Significant seasonal precipitation variations are only observed for areas west of the Cascades (Fig. A1). Since precipitation rates have a primary control on the hydrological cycle, this observation suggests that western streams are characterized by a more seasonally variable subsurface residence time distribution, whereas eastern streams show a less variable residence time distribution. Accordingly, the strong control of δ^7Li_{dis} by residence time accounts for the seasonal δ^7Li_{dis} variations observed in streams west of the Cascades and the lack of variations seen in eastern streams (Tables 1, 2).

The increase in δ^7Li_{dis} seen with an increasing river to subsurface residence time ratio (Fig. 6b) also explains why riverine δ^7Li_{dis} is generally greater than groundwater δ^7Li_{dis} (Fig. 7 and Tables 1 and 2). Accordingly, our observations and simulation results support the hypothesis that suspended river loads are reactive due to the presence of fine-grained primary silicate mineral particles, and therefore continued Li isotope fractionation is occurring within streams. This is also supported by a recent study of Lemarchand et al. (2010), who found δ^7Li_{dis} in streams draining a granitic catchment to be significantly greater than that of springs feeding these streams.

5.2. Climate control

There is no clear distinction in δ^7Li_{dis} values between western and eastern streams, suggesting that the amount of annual precipitation, and thus climatic conditions, do not have a direct influence on δ^7Li. This lack of climatic influence is consistent with the results of Millot et al. (2010), who suggested that neither mean annual precipitation nor distance to the coast have an influence on δ^7Li_{dis} in waters from the Mackenzie River basin. In addition, despite the large temperature difference between summer and late winter (~10 °C), there is no change in riverine δ^7Li_{dis} in eastern streams.

Interestingly, as discussed in the previous section, a clear seasonal control on δ^7Li_{dis} was observed for streams west of the Cascades (Fig. 5), which is probably related to the large seasonal difference in monthly precipitation observed there (Fig. A1). The proposal that average subsurface residence time is longer during drier periods is in good agreement with significantly larger TDS and [Si] observed for western streams during the summer compared to the winter (Table 1). A correlation between subsurface residence times and aqueous concentrations, and thus TDS, is expected because longer residence times allow for increased mineral dissolution and exchange (Fig. 6). Overall, climate indirectly affects δ^7Li as precipitation rates control the hydrological cycle and thus residence time distributions. However, δ^7Li is a poor proxy for climate because many other parameters affect the hydrological cycle as well (e.g., mountain building, pCO_2, temperature, vegetation).

5.3. δ^7Li as a tracer of chemical weathering

This study has illuminated the factors that control Li isotopic fractionation in the dissolved loads of rivers (δ^7Li_{dis}). Li isotopic fractionation in rivers is caused by fractionation between solution and secondary minerals (e.g., Huh et al., 2001, 1998; Pogge von Strandmann et al., 2010, 2006), and it has been suggested that the large variability in δ^7Li_{dis} may be partially caused by different fractionation factors associated with Fe–Mn oxyhydroxides in places without soils or clays (Millot et al., 2010; Wimpenny et al., 2010b). Our study shows that δ^7Li_{dis} is not simply controlled by mineral-specific fractionation, as there is no correlation

between δ^7Li_{dis} and SI of the oversaturated secondary minerals, such as hematite and kaolinite (Fig. A7). We have shown that parameters such as reservoir residence time and reaction between suspended and dissolved loads in rivers can significantly influence δ^7Li_{dis}, given a constant fractionation factor between solution and secondary minerals (Fig. 6), and there is no need (or evidence) to call upon variable fractionation factors related to the dominance of different secondary to explain variable δ^7Li_{dis} in rivers.

Our simulations (Fig. 6) agree very well with observations (Fig. 7), as we see a clear negative correlation between δ^7Li_{dis} and the Li/Na ratio, whereas, δ^7Li_{dis} does not correlate with [Si] or Si/TZ^+, and shows only a weak negative correlation with Li/TZ^+ (Fig. 6c). Based on our simulations and data, we infer that, with the exception of Li/Na, δ^7Li_{dis} and various silicate weathering proxies based on elemental concentrations (e.g., [Li], [Si], TZ^+) are only correlated when a natural system is dominated by either Li isotope fractionation occurring in the subsurface (in which case there is a positive correlation between δ^7Li_{dis} and the weathering proxies), or occurring in rivers (in which case there is a negative correlation between δ^7Li_{dis} and the proxies). If Li isotope fractionation occurs in both settings, there will be no correlation, as seen in our results. This finding may explain why correlations between δ^7Li_{dis} and concentration proxies are observed in some studies (e.g., Huh et al., 2001; Pogge von Strandmann et al., 2010), but not in others (this study; Millot et al., 2010).

Overall, this study also has implications for using Li isotopes as tracers of chemical weathering in rivers, and consequently, in seawater through time. In previous studies, multiple weathering proxies, such as [Si] and Si/TZ^+, [Li], combined with Li isotopes (e.g., Huh et al., 2001, 1998; Pogge von Strandmann et al., 2006), have been used to try to constrain silicate weathering intensity. However, correlations between δ^7Li_{dis} and these proxies may be produced or destroyed due to the effects we simulated, such as the residence time in the subsurface (as suggested in Millot et al., 2010), Li isotope fractionation and mineral dissolution in rivers. Our study suggests that δ^7Li_{dis} is more robust than other tracers of silicate weathering, because it is linked to the degree of water–rock interactions along a specific flow path (e.g., in the subsurface and in rivers). In general, the larger the δ^7Li_{dis} in a specific river, the more water–rock interactions (primary mineral dissolution + secondary mineral precipitations) have occurred such as shown by Wanner et al. (2014). We demonstrate that, in rivers draining single lithology catchments, δ^7Li_{dis} is negatively correlated with Li/Na, suggesting that the combined δ^7Li_{dis} vs. Li/Na plot (Fig. 7d) may be a sensitive indicator of the extent of chemical weathering occurring in streams and groundwater reservoirs. Moreover, this finding is observed globally by clear negative correlations between δ^7Li_{dis} vs. Li/Na for river waters worldwide that drain only or mainly basalts (Fig. 8). The global correlations observed in Fig. 8 is well related to our simulations (Fig. 6d), where we show that a perfect correlation is only observed for constant basalt [Li], which is clearly not the case when comparing basalts from the world over (e.g., [Li] = 3 to 23 ppm in fresh CRBs).

Finally, δ^7Li_{dis} is influenced by many hydrological parameters, so it is not straightforward to use δ^7Li_{dis} as a silicate weathering tracer in terms of interpreting secular evolution of riverine inputs to seawater. For example, for very fast flow at a high discharge, the overall silicate weathering rate (in moles/year) is very high. However, the δ^7Li value should remain low because of the short residence time. Assuming the rise in δ^7Li in seawater in the past 60 Ma (Misra and Froelich, 2012) is due primarily to changing riverine input with minor effects of discharge variations (Wanner et al., 2014), our work suggests that this signature reflects increased silicate weathering rates on the continents, which may or may not be directly related to changing climate (as we see no direct correlation between δ^7Li_{dis} and climate), but could well be due to tectonic uplift that causes an increase in water–rock reaction.

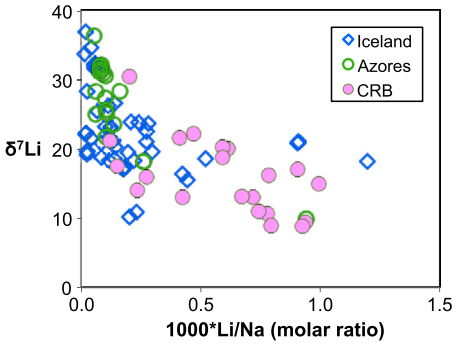

Fig. 8. δ^7Li versus 1000×Li/Na (molar ratio) in dissolved loads of streams and rivers draining basalts. Data are from this study, Pogge von Strandmann et al. (2006, 2010), and Vigier et al. (2006, 2009).

6. Conclusions

The main conclusions from this study are:

1. Large δ^7Li_{dis} variations (up to 20‰) are observed in streams that only drain basalts, suggesting that Li isotopic compositions in streams are controlled by factors other than the lithology of their catchments.
2. δ^7Li_{dis} is significantly higher than δ^7Li of groundwaters, suggesting that Li isotope fractionation occurring in rivers themselves play a major role on riverine δ^7Li_{dis}.
3. A lack of direct correlation between climatic conditions (i.e., mean annual precipitation, temperature) and riverine δ^7Li_{dis}, and correlations between seasonal precipitation variations and δ^7Li_{dis} suggest that subsurface residence times strongly influence riverine δ^7Li_{dis}.
4. Model simulations of reactive transport with variable residence times show that Li isotope fractionation occurs in both the subsurface and in rivers, causing many traditional silicate weathering proxies (e.g., [Si], Si/TZ^+) to show no, or only a weak correlation with δ^7Li_{dis}.
5. δ^7Li_{dis} and Li/Na in dissolved loads of rivers are only sensitive to the amount of water–rock interaction over time and are, thus, useful tracers of the degree of silicate chemical weathering occurring in single lithology catchments.
6. If the increase is δ^7Li in seawater through the Cenozoic is due primarily to changing riverine input, our results suggest that the increase may be uniquely related to tectonic uplift, which causes increased weathering due to the increase in denudation and the decreasing weathering intensity. Climatic controls on chemical weathering are apparently not as important.

Acknowledgements

We thank Richard Ash for assistance with the ICP-MS/MC-ICP-MS analyses, Igor Puchtel for help in the clean lab, Shuiwang Duan and Tammy Newcomer for major anion analyses, Terry Tolan for sampling guidance and discussion, Marshall Gannett, Steve Hinkle, Steve Cox, and Mike Free for help with fieldwork logistics, and Christie Galen for accompanying up in the field and showing us great birds. Sujay Kaushal kindly provided access to his Biogeochemistry laboratory and provided guidance on water sampling. We are grateful for discussions and comments from Jerome Gaillardet and Cin-Ty Lee. The manuscript benefited greatly from the review comments of three anonymous reviewers. Jean Lynch-Stieglitz is also thanked for her editorial handling and constructive

comments. This work was supported by a grant from the National Science Foundation (EAR 0948549 to RLR and WFM) and an Ann G. Wylie Dissertation Fellowship awarded to X-ML from the University of Maryland. X-ML acknowledges postdoctoral fellowship support from the Carnegie Institution of Washington. CW was supported by the U.S. Department of Energy, Geothermal Technologies Program, Energy Efficiency and Renewable Energy Office, Award No GT-480010-12.

Appendix A. Supplementary material

Supplementary material related to this article can be found online at http://dx.doi.org/10.1016/j.epsl.2014.10.032.

References

Basaltic Volcanism Study Project, 1981. Basaltic Volcanism on the Terrestrial Planets. Pergamon Press, Inc., New York. 1286 pp.

Berner, R.A., Lasaga, A.C., Garrels, R.M., 1983. The carbonate–silicate geochemical cycle and its effect on atmospheric carbon–dioxide over the past 100 million years. Am. J. Sci. 283, 641–683.

Blanc, P., Lassin, A., Piantone, P., Azaroual, M., Jacquemet, N., Fabbri, A., Gaucher, E.C., 2012. Thermoddem: a geochemical database focused on low temperature water/rock interactions and waste materials. Appl. Geochem. 27, 2107–2116.

Bouchez, J., Gaillardet, J., France-Lanord, C., Maurice, L., Dutra-Maia, P., 2011. Grain size control of river suspended sediment geochemistry: clues from Amazon River depth profiles. Geochem. Geophys. Geosyst. 12, Q03008. http://dx.doi.org/10.1029/2010GC003380.

Bouchez, J., von Blanckenburg, F., Schuessler, J.A., 2013. Modeling novel stable isotope ratios in the weathering zone. Am. J. Sci. 313, 267–308.

Brenan, J.M., Neroda, E., Lundstrom, C.C., Shaw, H.F., Ryerson, F.J., Phinney, D.L., 1998. Behaviour of boron, beryllium, and lithium during melting and crystallization: constraints from mineral-melt partitioning experiments. Geochim. Cosmochim. Acta 62, 2129–2141.

Brimhall, G.H., Lewis, C.J., Ford, C., Bratt, J., Taylor, G., Warin, O., 1991. Quantitative geochemical approach to pedogenesis – importance of parent material reduction, volumetric expansion, and eolian influx in lateralization. Geoderma 51, 51–91.

Chan, L.H., Edmond, J.M., Thompson, G., Gillis, K., 1992. Lithium isotopic composition of submarine basalts – implication for the lithium cycle in the oceans. Earth Planet. Sci. Lett. 108, 151–160.

Decarreau, A., Vigier, N., Pálková, H., Petit, S., Vieillard, P., Fontaine, C., 2012. Partitioning of lithium between smectite and solution: an experimental approach. Geochim. Cosmochim. Acta 85, 314–325.

Dessert, C., Dupré, B., Francois, L.M., Schott, J., Gaillardet, J., Chakrapani, G., Bajpai, S., 2001. Erosion of Deccan Traps determined by river geochemistry: impact on the global climate and the $^{87}Sr/^{86}Sr$ ratio of seawater. Earth Planet. Sci. Lett. 188, 459–474.

Flesch, G., Anderson, A., Svec, H., 1973. A secondary isotopic standard for $^{6}Li/^{7}Li$ determinations. Int. J. Mass Spectrom. Ion Phys. 12, 265–272.

Fryirs, K.A., Brierley, G.J., 2013. Geomorphic Analysis of River Systems: An Approach to Reading the Landscape. John Wiley & Sons.

Gaillardet, J., Dupré, B., Louvat, P., Allègre, C.J., 1999. Global silicate weathering and CO_2 consumption rates deduced from the chemistry of large rivers. Chem. Geol. 159, 3–30.

Hinkle, S.R., 1996. Age of ground water in basalt aquifers near Spring Creek National Fish Hatchery, Skamania County, Washington. U.S. Geological Survey Water-Resources Investigations Report. U.S. Fish and Wildlife Service, U.S. Dept. of the Interior.

Huh, Y., Chan, L.H., Zhang, L., Edmond, J.M., 1998. Lithium and its isotopes in major world rivers: implications for weathering and the oceanic budget. Geochim. Cosmochim. Acta 62, 2039–2051.

Huh, Y., Chan, L.H., Edmond, J.M., 2001. Lithium isotopes as a probe of weathering processes: Orinoco River. Earth Planet. Sci. Lett. 194, 189–199.

Kisakürek, B., Widdowson, M., James, R.H., 2004. Behaviour of Li isotopes during continental weathering: the Bidar laterite profile, India. Chem. Geol. 212, 27–44.

Kisakürek, B., James, R.H., Harris, N.B.W., 2005. Li and $\delta^{7}Li$ in Himalayan rivers: proxies for silicate weathering? Earth Planet. Sci. Lett. 237, 387–401.

Kohn, M.J., Miselis, J.L., Fremd, T.J., 2002. Oxygen isotope evidence for progressive uplift of the Cascade Range, Oregon. Earth Planet. Sci. Lett. 204, 151–165.

Lemarchand, E., Chabaux, F., Vigier, N., Millot, R., Pierret, M.C., 2010. Lithium isotope systematics in a forested granitic catchment (Strengbach, Vosges Mountains, France). Geochim. Cosmochim. Acta 74, 4612–4628.

Liu, X.-M., Rudnick, R.L., 2011. Constraints on continental crustal mass loss via chemical weathering using lithium and its isotopes. Proc. Natl. Acad. Sci. USA 108, 20873–20880.

Liu, X.-M., Rudnick, R.L., Hier-Majumder, S., Sirbescu, M.-L.C., 2010. Processes controlling lithium isotopic distribution in contact aureoles: a case study of the Florence County pegmatites, Wisconsin. Geochem. Geophys. Geosyst. 11, Q08014. http://dx.doi.org/10.1029/2010GC003063.

Liu, X.-M., Rudnick, R.L., McDonough, W.F., Cummings, M.L., 2013. Influence of chemical weathering on the composition of the continental crust: insights from Li and Nd isotopes in bauxite profiles developed on Columbia River Basalts. Geochim. Cosmochim. Acta 115, 73–91.

Magna, T., Wiechert, U.H., Halliday, A.N., 2004. Low-blank isotope ratio measurement of small samples of lithium using multiple-collector ICPMS. Int. J. Mass Spectrom. 239, 67–76.

Marschall, H.R., Pogge von Strandmann, P.A.E., Seitz, H.-M., Elliott, T., Niu, Y., 2007. The lithium isotopic composition of orogenic eclogites and deep subducted slabs. Earth Planet. Sci. Lett. 262, 563–580.

Millot, R., Vigier, N., Gaillardet, J., 2010. Behaviour of lithium and its isotopes during weathering in the Mackenzie Basin, Canada. Geochim. Cosmochim. Acta 74, 3897–3912.

Misra, S., Froelich, P.N., 2012. Lithium isotope history of cenozoic seawater: changes in silicate weathering and reverse weathering. Science 335, 818–823.

Négrel, P., Millot, R., Brenot, A., Bertin, C., 2010. Lithium isotopes as tracers of groundwater circulation in a peat land. Chem. Geol. 276, 119–127.

Nesbitt, H.W., Wilson, R.E., 1992. Recent chemical weathering of basalts. Am. J. Sci. 292, 740–777.

Piper, A.M., 1953. A Graphic Procedure in the Geochemical Interpretation of Water Analysis. U.S. Dept. of the Interior, Geological Survey, Water Resources Division, Ground Water Branch, Washington.

Pistiner, J.S., Henderson, G.M., 2003. Lithium-isotope fractionation during continental weathering processes. Earth Planet. Sci. Lett. 214, 327–339.

Pogge von Strandmann, P.A.E., Burton, K.W., James, R.H., van Calsteren, P., Gislason, S.R., Mokadem, F., 2006. Riverine behaviour of uranium and lithium isotopes in an actively glaciated basaltic terrain. Earth Planet. Sci. Lett. 251, 134–147.

Pogge von Strandmann, P.A.E., Burton, K.W., James, R.H., van Calsteren, P., Gislason, S.R., 2010. Assessing the role of climate on uranium and lithium isotope behaviour in rivers draining a basaltic terrain. Chem. Geol. 270, 227–239.

Qiu, L., Rudnick, R.L., McDonough, W.F., Merriman, R.J., 2009. Li and $\delta^{7}Li$ in mudrocks from the British Caledonides: metamorphism and source influences. Geochim. Cosmochim. Acta 73, 7325–7340.

Qiu, L., Rudnick, R.L., Ague, J.J., McDonough, W.F., 2011a. A lithium isotopic study of sub-greenschist to greenschist facies metamorphism in an accretionary prism, New Zealand. Earth Planet. Sci. Lett. 301, 213–221.

Qiu, L., Rudnick, R.L., McDonough, W.F., Bea, F., 2011b. The behavior of lithium in amphibolite- to granulite-facies rocks of the Ivrea–Verbano Zone, NW Italy. Chem. Geol. 289, 76–85.

Rudnick, R.L., Tomascak, P.B., Njo, H.B., Gardner, L.R., 2004. Extreme lithium isotopic fractionation during continental weathering revealed in saprolites from South Carolina. Chem. Geol. 212, 45–57.

Singleton, M.J., Sonnenthal, E.L., Conrad, M.E., DePaolo, D.J., Gee, G.W., 2005. Multiphase reactive transport modeling of seasonal infiltration events and stable isotope fractionation in unsaturated zone pore water and vapor at the Hanford site. Vadose Zone J. 3, 775–785.

Sonnenthal, E., Spycher, N., Apps, J., Simmons, A., 1998. Thermo-hydro-chemical predictive analysis for the Drift-Scale Heater Test. Yucca Mountain Project, Level 4.

Takeuchi, A., Hren, M.T., Smith, S.V., Chamberlain, C.P., Larson, P.B., 2010. Pedogenic carbonate carbon isotopic constraints on paleoprecipitation: evolution of desert in the Pacific Northwest, USA, in response to topographic development of the Cascade Range. Chem. Geol. 277, 323–335.

Taylor, A.S., Lasaga, A.C., 1999. The role of basalt weathering in the Sr isotope budget of the oceans. Chem. Geol. 161, 199–214.

Teng, F.Z., McDonough, W.F., Rudnick, R.L., Dalpe, C., Tomascak, P.B., Chappell, B.W., Gao, S., 2004. Lithium isotopic composition and concentration of the upper continental crust. Geochim. Cosmochim. Acta 68, 4167–4178.

Teng, F.Z., McDonough, W.F., Rudnick, R.L., Wing, B.A., 2007. Limited lithium isotopic fractionation during progressive metamorphic dehydration in metapelites: a case study from the Onawa contact aureole, Maine. Chem. Geol. 239, 1–12.

Vigier, N., Burton, K.W., Gislason, S.R., Rogers, N.W., Duchene, S., Thomas, L., Hodge, E., Schaefer, B., 2006. The relationship between riverine u-series disequilibria and erosion rates in a basaltic terrain. Earth Planet. Sci. Lett. 249, 258–273.

Vigier, N., Gislason, S.R., Burton, K.W., Millot, R., Mokadem, F., 2009. The relationship between riverine lithium isotope composition and silicate weathering rates in Iceland. Earth Planet. Sci. Lett. 287, 434–441.

Wanner, C., Sonnenthal, E.L., 2013. Assessing the control on the effective kinetic Cr isotope fractionation factor: a reactive transport modeling approach. Chem. Geol. 337, 88–98.

Wanner, C., Sonnenthal, E.L., Liu, X.-M., 2014. Seawater $\delta^{7}Li$: a direct proxy for global CO_2 consumption by continental silicate weathering? Chem. Geol. 381, 154–167.

Wimpenny, J., Gislason, S.R., James, R.H., Gannoun, A., Pogge Von Strandmann, P.A.E., Burton, K.W., 2010a. The behaviour of Li and Mg isotopes during primary phase

dissolution and secondary mineral formation in basalt. Geochim. Cosmochim. Acta 74, 5259–5279.
Wimpenny, J., James, R.H., Burton, K.W., Gannoun, A., Mokadem, F., Gislason, S.R., 2010b. Glacial effects on weathering processes: new insights from the elemental and lithium isotopic composition of West Greenland rivers. Earth Planet. Sci. Lett. 290, 427–437.
Xu, T., Spycher, N., Sonnenthal, E.L., Zhang, G., Zheng, L., Pruess, K., 2011. TOUGHREACT Version 2.0: a simulator for subsurface reactive transport under non-isothermal multiphase flow conditions. Comput. Geosci. 37, 763–774.
Zhang, L.B., Chan, L.H., Gieskes, J.M., 1998. Lithium isotope geochemistry of pore waters from Ocean Drilling Program Sites 918 and 919, Irminger Basin. Geochim. Cosmochim. Acta 62, 2437–2450.